

EVALUATING INTERFEROMETRIC BASELINE PERFORMANCES IN A CLOSE FORMATION FLIGHT BY USING GRACE GPS NAVIGATION SOLUTIONS

A.O. Kohlhase, S. D'Amico
German Space Operations Center (GSOC)
DLR Oberpfaffenhofen, 82234 Weßling, Germany
(E-mail : andreas.kohlhase@dlr.de, simone.damico@dlr.de)

R. Kroes
Department of Earth Observation and Space Systems (DEOS)
TU Delft, Kluywerweg 1, 2926 Delft, The Netherlands
(E-mail: r.kroes@lr.tudelft.nl)

Abstract

In this paper the impact of relative position errors on the interferometric baseline performance of multistatic Synthetic Aperture Radar (SAR) satellites flying in a close formation is analyzed and assessed. Based on accuracy results obtained from differential GPS (DGPS) observations between the twin Gravity Recovery and Climate Experiment (GRACE) satellites, baseline uncertainties are derived for three interferometric scenarios of a dedicated SAR mission. To assess the accuracy with respect to quality requirements of high-resolution DEMs, topographic height errors are derived from the estimated baseline uncertainties. The analysis reveals that the induced low-frequency modulation (height bias) fulfills the relative vertical accuracy requirement ($\sigma < 1$ m linear point-to-point error) of a Digital Terrain Elevation Data model of level 3 (DTED-3) for most of the baseline constellations. DGPS can be used as an operational navigation tool for high-precise baseline estimation if a geodetic-grade dual-frequency spaceborne GPS receiver is assumed to be the primary instrument onboard the SAR satellites. To exemplarily demonstrate the error propagation into the interferogram Orbital Phase Screens (OPS) are generated by differencing simulated interferograms. These are calculated from baselines of distinct GRACE error signatures and magnitudes.

1. Introduction

The accurate digital mapping of the world's topography using synthetic aperture radar (SAR) interferometry

is still a major topic in Earth remote sensing (e.g., [1] [2]). This geodetic technique is based on the combination of two SAR images of the same scene acquired from slightly different positions in space to measure a phase difference in each co-registered pixel. The measured interferometric phase can be used to derive topographic height information on the imaged terrain and thus to generate a digital elevation model (DEM) (e.g., [3]). The precision of the height estimation is primarily determined by the size of the satellite to satellite baseline and the accuracy of its reconstruction, as well as the quality of the interferometric phase correlation.

The baseline length is one of the main driving parameters for the performance and mainly determines the vertical accuracy of the estimated DEM. A solution to overcome this problem is thus to define a satellite constellation allowing for varying and multiple baselines to acquire two or more SAR images of the same scene quasi-simultaneously. In addition, if one SAR sensor is transmitting and receiving, whereas the other ones only receive the radar echoes, the interferometric measurement becomes less sensitive to phase ambiguities. This approach is called multistatic single-pass SAR interferometry. An important parameter to quantify the sensitivity is the so-called height or altitude of ambiguity. This height corresponds to exactly one interferometric phase cycle $[0, 2\pi]$ of range change between the SAR sensor and a reflector on the ground. In other words, if a terrain elevation exceeds the altitude of ambiguity the measurement becomes ambiguous. The principle observation is thus a two-dimensional relative phase signal, which is the 2π -modulus of the (unknown) absolute phase signal [4].

To analyze the performance of a multistatic SAR system comprehensively, we need to estimate the interferometric phase and baseline errors. Both errors can be propagated into so-called topographic or interferometric height

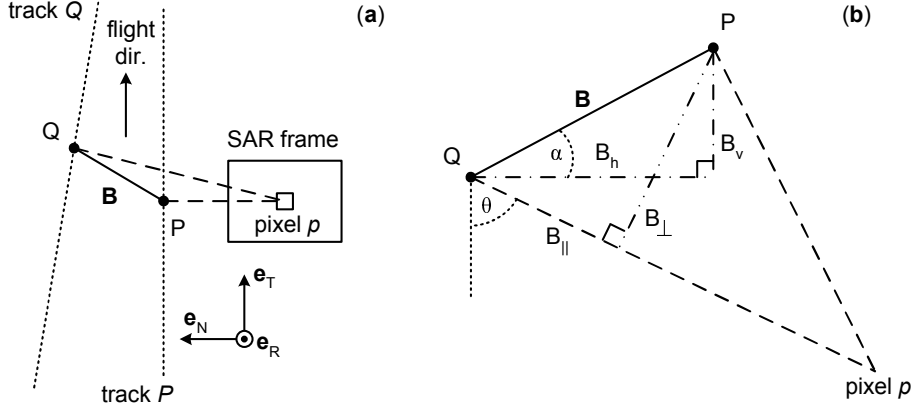


Figure 1: **(a)** The baseline is formed at the moment of alignment of a coregistered pixel p . Here points P and Q resemble the positions of the S/C at the moment of alignment for the different scenarios, listed in Table 1. **(b)** Two possible representations of the interferometric baseline: horizontal/vertical or parallel/perpendicular.

errors, which determines the vertical resolution and precision of a DEM. For multistatic SAR configurations, the influence of interferometric phase errors on the height accuracy has already been analyzed by [5]. However, the specific performance under the condition of rapidly changing multistatic baseline conditions requires a detailed analysis in so far as the achievable baseline accuracy changes for different baseline determination strategies.

In the following, we analyze and assess the achievability of a stated DEM accuracy requirement by deriving height biases from baseline errors. We use GPS positioning results from the global recovery and climate experiment (GRACE) mission (e.g., [6]) to estimate the baseline errors for different interferometric scenarios of a dedicated SAR mission. Here, the availability of the K-band radar link provides a unique operation for validating GPS-based relative positions at the sub-mm level. In this way, realistic accuracy estimates can be derived that are free of simplifying assumptions made in earlier software and hardware-in-the-loop simulation [7].

2. Performance requirements and basic assumptions

To analyze the baseline performance of an exemplary multistatic SAR interferometer in more detail, we use the main system specifications of the proposed TanDEM-X mission in which two main interferometric scenarios are defined for DEM generation [2]: the bistatic and the monostatic pursuit mode. In the bistatic mode, the SAR instrument of the master satellite will be active (transmitting and receiving), whereas the one on the slave satellite will be passive (only receiving). This counteracts the problem of the inherent accuracy limitation due to temporal decorrelation and atmospheric disturbances. In the monostatic mode, one satellite pursues the other with a

Table 1: Physical representation of the points P and Q in Fig. 1 for the different interferometric scenarios.

Scenario	P		Q	
	S/C	Epoch	S/C	Epoch
Bistatic	A	t_0	B	t_0
Monostatic pursuit	A	$t_0 + \Delta t$	B	t_0
Repeat-pass	A	t_1	A	t_2

selectable along-track separation. This ensures independent work of both instruments, i.e., both SAR antennas will transmit and receive. Furthermore, a repeat-pass scenario for the prime satellite is taken into account.

2.1 Definition of baseline geometry

The baseline geometry for the two SAR acquisition modes and for the repeat-pass scenario is explained using Fig. 1. Here points P and Q resemble the different spacecraft positions for each scenario at the moment when the co-registered pixels of the SAR frames are aligned (Fig. 1a). The baseline

$$\mathbf{B} = [B_R, B_T, B_N]^T \quad (1)$$

is a 3-D relative position between these points and is usually defined in the co-rotating coordinate system, in which the unit vector \mathbf{e}_R points in radial, \mathbf{e}_T in tangential (along-track), and \mathbf{e}_N in normal (cross-track) direction (Fig. 1a). \mathbf{B} thus consists of a radial, B_R , an along-track, B_T , and a cross-track component B_N .

The baseline can be displayed in a 2-D plane stretched between the pixel p and points P and Q (Fig. 1b). Both baseline representations may simply be converted to each other by using the radar look angle θ , which is defined with respect to the geocentric state vector of a spacecraft in point Q. The attitude or tilt angle α is used to describe the orientation of the baseline with respect to the horizon.

The exact meanings of points P and Q for the different scenarios can be found in Table 1.

In this study, the estimation of the baseline error is the primary concern. Baseline errors in the tangential direction, σ_{B_T} , are usually corrected for sufficiently during SAR frame alignment. Only the errors in cross-track and radial direction propagate as phase errors into the interferogram, making it essentially a 2-D problem. In the following, the (B_N, B_R) -representation is used since errors in the horizontal and vertical component of the baseline can directly be related to the cross-track and radial orbit errors, respectively. Hence

$$\sigma_{B_N} = \sigma_{B_h} \quad \text{and} \quad \sigma_{B_R} = \sigma_{B_v} \quad (2)$$

2.2 DEM vertical accuracy requirements

For the TanDEM-X mission, a baseline induced height bias screen is claimed which has to be compliant with the relative vertical accuracy according to the digital terrain elevation data level 3 (DTED-3) specifications. The stated accuracy objective is < 2 m linear point-to-point error at 90% probability for flat terrains. This allows the assumption of a relative vertical accuracy of roughly < 1 m linear point-to-point error at 68.3% (1σ) probability. Since the radar is always side-looking, terrain elevation will result in geometric distortions in the SAR image due to the varying incidence angle.

To find a trade-off between a high signal-to-noise ratio (SNR) and reduced distortion effects, the SAR satellites will map the scene under different radar look angles, which also has to be accounted for in the performance analysis. For this analysis, it is assumed that errors in the interferometric phase and bistatic focusing can be modeled precisely, which is important for the separation between the baseline and purely phase noise induced height bias in each DEM point.

2.3 Prediction of relative motion

In order to predict the relative motion of two satellites in space and thus to have a priori information of the baseline vector, a possible approach is to numerically integrate the differential equations of motion of both objects in the presence of all relevant perturbations. We choose the initial values in such a way that the characteristic formation flight is reached as described in [8]. To minimize the risk of collision, care is taken to properly separate the two spacecrafts in radial and cross-track directions. This is achieved by a parallel (or anti-parallel) alignment of the relative eccentricity and inclination vectors.

Both TanDEM-X satellites will orbit the Earth in nearly circular and sun synchronous orbits. A difference in the right ascension of the ascending nodes ensures a horizontal offset in the equatorial region, whereas a slight difference in the eccentricities allows for a minimal vertical displacement in polar regions. The 2-D baseline vector is simply formed by using the radial/cross-track representation of the differenced state vectors at a certain epoch.

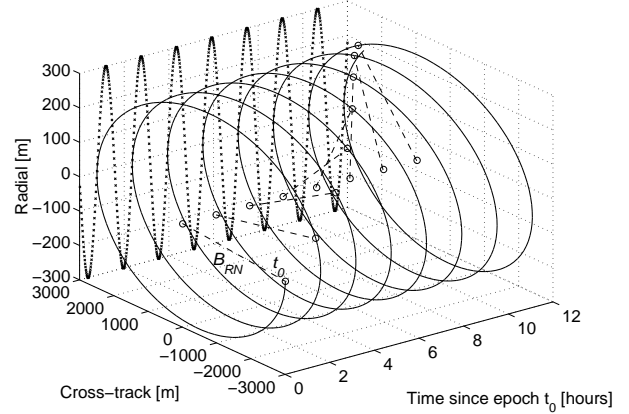


Figure 2: 3-D representation of motion of the baseline vector \mathbf{B}_{RN} .

The prediction yields a baseline length of roughly 300 m for the vertical attitude ($\alpha = 90^\circ$) and 3000 m for the horizontal orientation ($\alpha = 0^\circ$), see Fig. 2. The dynamical behavior of the resulting interferometric baseline can be characterized by a so-called Helix rotation with a fluctuating length.

As shown in [8], such a formation-flying configuration is naturally stable over short-term prediction arcs (i.e., hours). For long-term formation flying (i.e., days), a relative orbit control of the formation is necessary in order to counteract differential perturbations mainly caused by the Earth's oblateness (i.e., J_2 effects) and differential atmospheric drag.

3 Performance of baseline determination strategies

For the following baseline determination strategies, a geodetic-grade dual-frequency spaceborne GPS receiver, such as the JPL BlackJack GPS receiver, is assumed to be the primary instrument for POD onboard the SAR satellites.

3.1 Repeat-pass interferometry

Since the same satellite takes SAR images after a defined repeat cycle, the interferometric baseline

$$\mathbf{B} = \mathbf{r}_A(t_2) - \mathbf{r}_A(t_1) \quad (3)$$

is thus formed from two absolute positions (Fig. 1) of the satellite at epochs t_1 and t_2 . The baseline error

$$\epsilon_{\mathbf{B}} = \epsilon_{\mathbf{r}_A}(t_2) - \epsilon_{\mathbf{r}_A}(t_1) \quad (4)$$

results from the individual errors of both satellite passes. For long time scales, there is no temporal correlation between the errors of the repeat-pass position vector \mathbf{r}_A .

Table 2: Comparison of absolute orbit solutions for GRACE A and B computed at DLR and JPL for 2003 DOY 210 - 220 (July 29 - August 8).

DOY	GRACE A / B		
	$\sigma_R(\text{cm})$	$\sigma_T(\text{cm})$	$\sigma_N(\text{cm})$
210	2.1 / 2.2	3.9 / 3.8	2.1 / 1.9
211	2.3 / 2.3	4.1 / 4.1	2.2 / 2.1
212	2.4 / 2.7	4.3 / 4.5	1.8 / 1.6
213	2.1 / 2.2	3.3 / 3.8	2.7 / 1.8
214	2.2 / 2.3	4.2 / 4.1	2.9 / 1.8
215	2.0 / 2.3	3.8 / 4.1	2.7 / 2.2
216	2.1 / 2.2	4.2 / 4.1	2.4 / 1.8
217	1.9 / 2.1	3.2 / 3.5	2.7 / 2.0
218	2.2 / 2.1	4.0 / 3.9	2.0 / 1.9
219	1.9 / 2.3	3.4 / 4.0	2.5 / 1.7
220	1.9 / 2.3	3.1 / 4.0	1.9 / 1.8
Avg.	2.2	3.9	2.1

The inaccuracies of both absolute positions are simply propagated into the uncertainty of the baseline length

$$\sigma_B = \sqrt{\sigma_{\mathbf{r}_A}^2(t_2) + \sigma_{\mathbf{r}_A}^2(t_1)} = \sqrt{2} \sigma_{\mathbf{r}_A}. \quad (5)$$

Realistic accuracies for GPS-based absolute orbits are obtained from an orbit comparison of the GRACE mission found in Table 2, which shows the difference between the absolute orbit solutions computed for this study at the Deutsche Zentrum für Luft- und Raumfahrt (DLR) and the Jet Propulsion Laboratory (JPL) solutions of GRACE A and B, respectively, in radial, along-track and cross-track direction. The JPL orbit solution is distributed with the publicly available GRACE data [9]. The DLR orbits have been computed using the reduced dynamic batch least-squares estimation process [10], using both GPS code pseudorange and carrier-phase data. The difference among solutions from several institutes gives a good indication of the overall orbit accuracy. Here, the overall orbital errors are obtained as roughly 2 cm in radial and cross-track directions and 4 cm in the along-track direction.

Expressing Eq. (5) in terms of mean uncertainties in radial and cross-track direction, a 2-D baseline uncertainty

$$\sigma_B = \sqrt{2(\bar{\sigma}_R^2 + \bar{\sigma}_N^2)} \quad (6)$$

of 4.3 cm may be estimated for a repeat-pass scenario using absolute GPS navigation solutions for post-facto orbit reconstruction.

3.2 Bistatic mode

For this scenario, the interferometric baseline

$$\mathbf{B} = \Delta \mathbf{r}_{\text{DGPS}}(t_0) \quad (7)$$

is identical with the observation of relative position between both satellites according to Fig. 1. A study by [11] using data from the GRACE mission has shown that

DGPS can also be successfully applied for precise relative positioning of formation-flying satellites. The unique aspect of the GRACE mission is that the accuracy of the along-track component of the relative position can be verified precisely with data from the KBR. Table 3 shows the uncertainties of the GRACE relative position compared to KBR data. For completeness, the relative position has been computed directly using DGPS data and by simply subtracting the absolute positions of both spacecrafts.

As can be seen from Table 3, the direct processing of DGPS data yields the highest accuracy of typically 1 mm in along-track direction. Simply subtracting two individual absolute orbit solutions does not give the desired accuracy, but still shows that the orbit errors of the individual satellites are highly correlated within the formation. This can be seen by comparing the accuracies in Tables 2 and 3 where, especially, the difference in the uncertainty of the along-track component is clearly visible.

Figure 3 shows the error of the GRACE relative position, $\epsilon_{\Delta \mathbf{r}}$, estimated using the DGPS filter described in [11] in comparison with data from the KBR. Also shown in Fig. 3 is the filter formal error in along-track direction. The 1σ value of the true error is 1 mm, which is close to the filter prediction of 0.6 mm. The DGPS filter shows the same formal error for the radial, along-track, and cross-track direction and it is therefore assumed that the true error for each component is also identical for all axes, resulting in a mean 2-D baseline uncertainty

$$\sigma_B = \sqrt{\bar{\sigma}_{\Delta r_R}^2 + \bar{\sigma}_{\Delta r_N}^2} = \sqrt{2} \bar{\sigma}_{T, \text{DGPS}} \quad (8)$$

of 1.4 mm for a bistatic scenario.

Since the relative distance of the TanDEM-X satellites in the bistatic formation flight is much smaller (< 3 km) than for GRACE (~ 220 km), an increase in baseline accuracy might be expected. However, this is not the case since the baseline solution is most likely dominated by errors independent of the separation, such as GPS signal multipath. A shorter separation, however, will increase the robustness of the solution. First of all, a larger number of GPS satellites will be jointly observed by both GPS receivers, leading to a reduced number of DGPS data outages. Second, and more important, when using dual-frequency GPS receivers, the double difference integer carrier-phase ambiguities can be determined with a much higher reliability due to the quasi elimination of the relative ionosphere, which dramatically strengthens the relative position solution.

3.3 Monostatic pursuit mode

In the monostatic pursuit mode of the TanDEM-X mission, the satellite formation has an along-track separation of 30-50 km, which can be represented by the baseline geometry sketched in Fig. 1. This means that spacecraft A in point P pursues spacecraft B in point Q with a time offset of $\Delta t \approx 4 - 7$ seconds. In this case,

Table 3: Comparison of the relative orbit solution for GRACE A and B, from the absolute orbits and by direct differential GPS processing.

DOY	GPS (DLR - JPL)			GPS (JPL - KBR)	GPS (DLR - KBR)	DGPS (DLR - KBR)
	σ_R (mm)	σ_T (mm)	σ_N (mm)	σ_T (mm)	σ_T (mm)	σ_T (mm)
210	10.3	24.0	14.6	16.1	14.4	1.03
211	13.6	24.7	15.0	17.6	15.9	0.82
212	10.5	22.5	13.8	17.7	14.5	0.81
213	11.2	21.5	20.1	16.4	10.6	1.20
214	10.9	24.6	27.3	16.0	13.3	0.86
215	13.4	30.5	16.2	16.4	22.6	1.03
216	9.1	36.7	18.8	18.3	21.0	0.72
217	11.1	23.2	19.9	17.6	13.9	1.41
218	9.9	21.7	14.6	18.3	13.8	0.95
219	11.5	22.1	26.0	19.5	12.1	0.81
220	12.7	26.1	22.5	17.8	16.9	1.19
Avg.	11.3	25.2	19.0	17.4	15.4	0.98

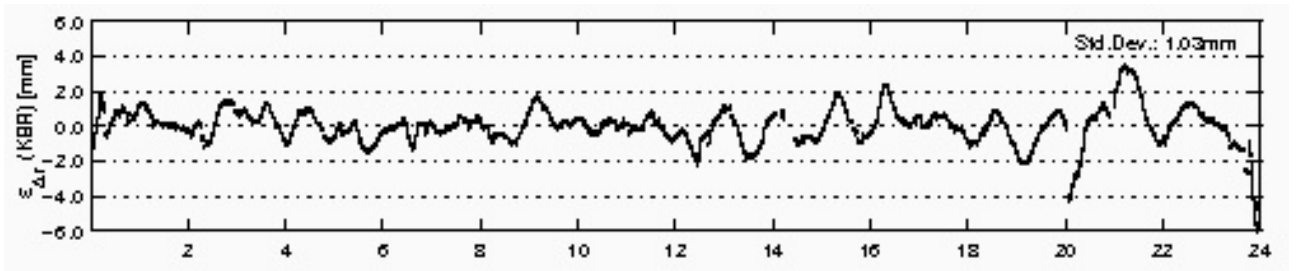


Figure 3: For 2003 DOY 215: True GRACE relative position error, $\epsilon_{\Delta r}$, from the DGPS filter verified using KBR data.

the interferometric baseline may be expressed as

$$\mathbf{B} = \mathbf{r}_A(t_0 + \Delta t) - \mathbf{r}_B(t_0) \quad (9)$$

which looks similar to the repeat-pass case according to Eq. (3).

Due to the relatively short inter-satellite separation, the relative spacecraft position could still be computed directly using DGPS data and with the same accuracy as described above. However, the difference in Eq. (9) is not measured by DGPS. At any given time, t , the position of spacecraft A can be expressed as the position of spacecraft B and the observed relative spacecraft position $\Delta \mathbf{r}_{\text{DGPS}}$ yielding

$$\mathbf{r}_A(t) = \Delta \mathbf{r}_{\text{DGPS}}(t) + \mathbf{r}_B(t). \quad (10)$$

By combining Eqs. (9) and (10), the interferometric baseline at $t = t_0 + \Delta t$ now becomes

$$\mathbf{B} = \Delta \mathbf{r}_{\text{DGPS}}(t_0 + \Delta t) + \mathbf{r}_B(t_0 + \Delta t) - \mathbf{r}_B(t_0) \quad (11)$$

which means that $\mathbf{r}_B(t_0 + \Delta t) - \mathbf{r}_B(t_0)$ yields an additional error due to absolute orbit reconstruction uncertainties between epochs t_0 and $t_0 + \Delta t$. For short time intervals, the errors of the reduced dynamic satellite orbit have a high degree of temporal correlation, and thereby reduce the interferometric baseline error in this case to

$$\epsilon_{\mathbf{B}} = \epsilon_{\Delta r}(t_0 + \Delta t) + \frac{\partial \epsilon_{\mathbf{r}}}{\partial t} \Delta t. \quad (12)$$

Analyzing the orbit data used to create Table 2, it was found that the orbital errors in each direction change over short periods of time with a maximum rate, $\partial \epsilon_{\mathbf{r}} / \partial t$, of 0.05 mm/s. For a maximum time interval of 8 seconds, this means a maximum error of 0.4 mm in the difference of the absolute GRACE positions for each component. Combining this with the average accuracy of the relative position solution, the resulting baseline will have a maximum mean 2-D uncertainty

$$\sigma_B = \sqrt{2 (\bar{\sigma}_{T,\text{DGPS}}^2 + \sigma_{(\partial \epsilon / \partial t) \Delta t}^2)} \quad (13)$$

of approximately 1.7 mm for a monostatic formation flight with a time offset of 8 seconds in flight direction.

4. Performance analysis

To investigate and assess the baseline performance for the bistatic and monostatic pursuit mode under quasi realistic conditions, i.e. to simulate the Helix baseline rotation, we use the two orbit predictions for the tandem formation flight which are based on fully dynamic trajectory modeling (Sect.). The cross-track baseline vector, \mathbf{B}_{RN} , can now be determined as a function of time since t_0 or the tilt angle α using both orbit predictions. The baseline

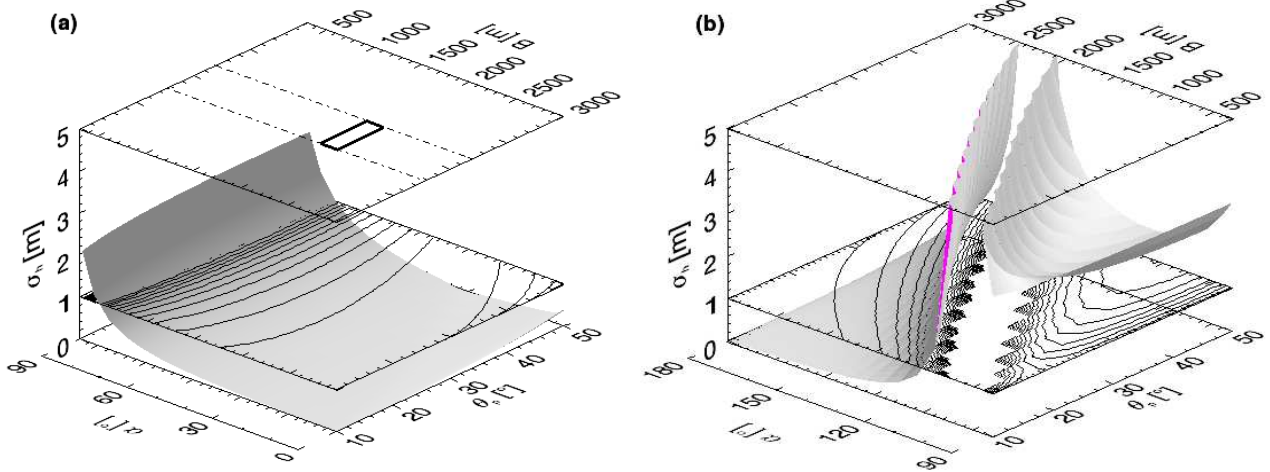


Figure 4: 3-D plots of relative topographic height errors σ_h as a function of the radar look angle θ_p and the baseline length B in case of the monostatic pursuit mode. (a) Estimated performance for baseline attitudes $\alpha \in [0, 90^\circ]$ assuming a mean satellite altitude of $H = 520$ km and a mean baseline standard deviation of $\sigma_B = 1.7$ mm. (b) Estimated relative height errors for baseline attitudes $\alpha \in (90^\circ, 180^\circ]$.

estimate applies both for the bistatic and the monostatic case.

We will consider the estimated baseline uncertainty for the monostatic operational mode as the *worst case* for the performance assessment. In other words, if the monostatic baseline performance fulfills the required DEM accuracy, the same must be true for the bistatic case for which we expect a slightly decreased baseline standard deviation (Sect.). The baseline error is propagated to topographic height errors using

$$\sigma_h = \left| -\frac{H_p}{B} \tan(\theta_p - \alpha) \tan \theta_p \right| \sigma_B \quad (14)$$

where H_p denotes the satellite's altitude above the terrain at target point P . Note that locally induced height errors due to changes of terrain elevation are neglected. However, Eq. (14) can be used for a reliable priori performance estimation.

The results are plotted in Figure 4. The estimated relative height error σ_h is expressed as function of radar look angle θ_p and the baseline length B , which is directly related to the tilt angle α due to baseline dynamics. θ_p is an independent parameter and varied between 10 and 50° at each predicted epoch to account for varying geometric distortion effects induced by different terrains.

During the first quarter-rotation $\alpha \in [0, 90^\circ]$, the baseline contracts from 3000 to 300 m (Fig. 4a). The induced height bias is always beneath the 1 m-performance threshold up to a tilt angle of roughly $\alpha = 85^\circ$. The bias raises slightly with increasing look angle. Figure (4a) confirms the low-frequency modulation of the topographic height bias that would occur for an interferometric measurement using ScanSAR pairs of a maximal acquisition window (rectangle with bold lines).

In the second quarter-rotation $\alpha \in (90^\circ, 180^\circ]$, the base-

line extends from 300 to 3000 m (Fig. 4b). Here, the performance is mostly corrupted by the singularity event at $\theta_p - \alpha = 90^\circ$. Only the noise levels occurring for baseline lengths $B \in [800, 3000$ m] at $\theta_p = 10^\circ$ and $B \in [2500, 3000$ m] at $\theta_p = 50^\circ$ are tolerable.

To assess the baseline performance, the estimated height bias in each DEM point p is related to the corresponding height ambiguity h_a , which is also a function of the parameters B , θ_p and α . It can be formulated as

$$h_a = \left| \frac{\lambda H_p}{m B_{\perp,p}} \tan \theta_p \right| \quad m = 1, 2 \quad (15)$$

with the effective baseline $B_{\perp,p} = B \cos(\theta_p - \alpha)$. λ denotes the radar wavelength (3.1 cm for X-band). The SAR acquisition parameter m has to be set to $m = 1$ for multistatic acquisition and to $m = 2$ for monostatic data takes.

Using the same baseline predictions as for the analysis in Fig. 4a and Eq. (15), we find the lowest height ambiguity $h_a \approx 1$ m for $\theta_p = 10^\circ$, $B = 3000$ m and the highest level $h_a \approx 73$ m for $\theta_p = 50^\circ$, $B = 300$ m. If the SAR data are acquired in the monostatic mode ($m = 2$), the height ambiguities are halved, which doubles the sensitivity of the interferometric measurement to relief.

5. First simulation results

To demonstrate the error propagation into an interferogram we generate so-called Orbital Phase Screens (OPS) by differencing simulated interferograms. These are calculated from state vectors and for the monostatic acquisition mode ($m = 2$). The interferometric phase Φ in each

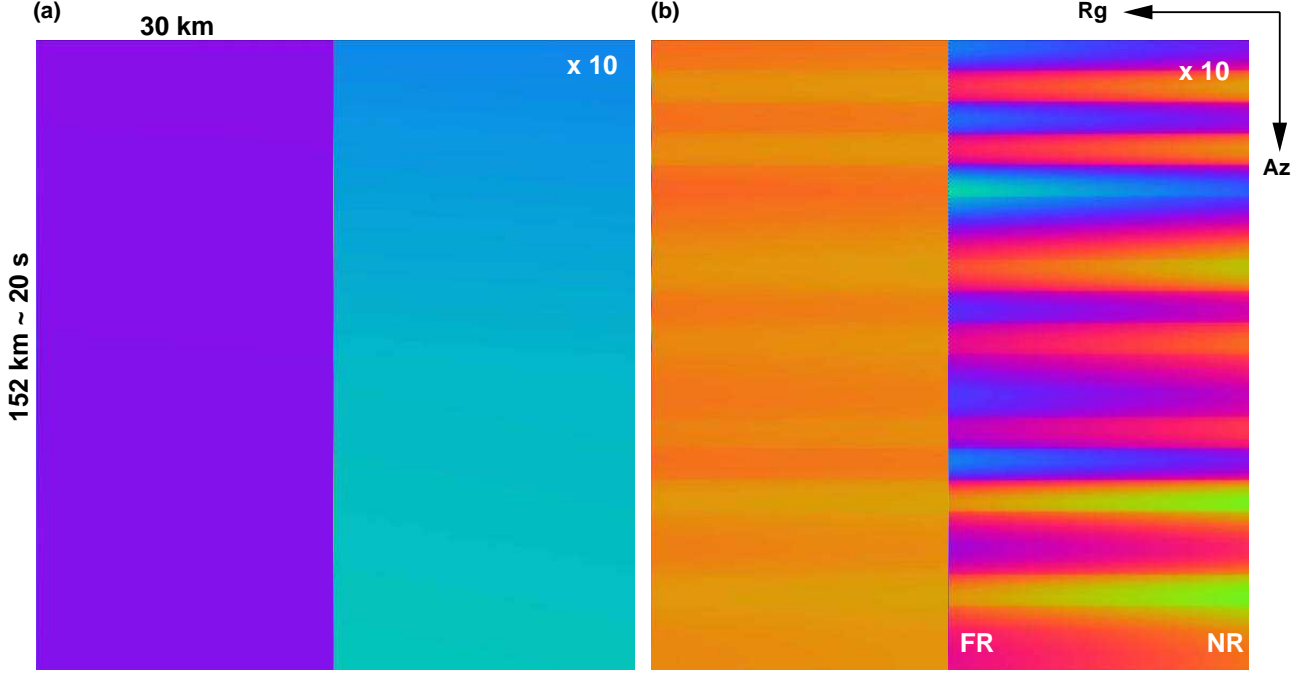


Figure 5: Interferometric x-Band simulations results. **(a)** OPS obtained from true GRACE relative position errors. **(b)** OPS obtained from the difference of the absolute GRACE A/B DLR and JPL orbit solution.

pixel p can be expressed as

$$\Phi_p = \varphi_{Ap} - \varphi_{Bp} = -\frac{4\pi}{\lambda} \Delta\rho \quad (16)$$

where $\Delta\rho$ is the difference of the 2 ranges in the line of sight. The range differences are estimated from the position vectors at each epoch and from the corresponding geodetic coordinates of the target points in the modeled topography. The mean satellite altitude is about 514 km. We apply the equation system

$$\begin{aligned} \mathbf{r}_1(t) &= \mathbf{r}_{1,0}(t) \\ \mathbf{r}_{1e}^{(rtn)}(t) &= \mathbf{M} \times \mathbf{r}_1(t) + \epsilon_n^{(rtn)}(t) \\ \mathbf{r}_2^{(rtn)}(t) &= \mathbf{M} \times \mathbf{r}_1(t) + \mathbf{B}^{(rtn)}(t) \\ \mathbf{r}_{2e}^{(rtn)}(t) &= \mathbf{r}_2^{(rtn)}(t) + \epsilon_n^{(rtn)}(t) \quad n = 1, 2 \end{aligned} \quad (17)$$

to calculate the position vectors for the second and third short-arc orbit. e indicates the erroneous position vector. \mathbf{M} is the matrix to transform the vectors from the Earth-fixed reference system into the co-rotating rtn -system. We define a constant baseline $\mathbf{B} = [10 m, 0, 0]^T$ according to Eq. 1. The first error vector is formed by using the true GRACE relative position errors as plotted in Fig. 3:

$$\epsilon_1 = [\epsilon_{\Delta r}(t), 0, \epsilon_{\Delta r}(t + \Delta T)]^T. \quad (18)$$

The second one is derived from the difference of the absolute DLR and JPL orbit solutions yielding

$$\epsilon_2 = [\epsilon_R(t), 0, \epsilon_N(t + \Delta T)]^T. \quad (19)$$

To statistically decorrelate the error components in radial and normal direction, we use the same data set for

each error estimation but take normal components of a 1-hour later epoch. We choose a 60s short-arc to calculate an interferogram of an about 150km-long scene in flight/Azimuth-direction ($\sim 20s$ short-arc length) containing position vectors with a 1s time interval. To synchronize the 10s sampling rate of the DGPS solution with the time step of the satellite position vectors, we interpolate the DGPS error vectors to obtain 1s steps. After re-transformation

$$\mathbf{r}_m = \mathbf{M}^{-1} \times \mathbf{r}_m^{(rtn)} \quad m = 1e, 2, 2e \quad (20)$$

we obtain the position vectors necessary for interferometric SAR processing.

We are now able to calculate $\Phi_{p,12}$ and $\Phi_{p,12e}$ containing the interferometric error phase induced by the relative position errors. Using the second error vector yields the second perturbed interferogram $\Phi_{p,1e2e}$ which is calculated from the position vectors with absolute errors. Normally, an interferometric measurement comprises several phase contributions. In our case, the simulated phase can be written as

$$\Phi_p = \Phi_{p,topo} + \Phi_{p,noise} + \Phi_\epsilon. \quad (21)$$

The topographic phase $\Phi_{p,topo}$ is estimated by using a standard reference ellipsoid. The interferometric phase noise is set to $\Phi_{p,noise} = 0$. Differencing the simulated interferograms again

$$\begin{aligned} \Delta\Phi_{p,1} &= \Phi_{p,12} - \Phi_{p,12e} \\ \Delta\Phi_{p,2} &= \Phi_{p,12} - \Phi_{p,1e2e} \end{aligned} \quad (22)$$

yields the pure orbital phase error or the OPS. The results are shown in Fig. 5

To better see the phase signals, we amplify them by a factor of 10. Here, one color cycle corresponds to one phase cycle $[0, 2\pi]$. Even with a baseline length of 10 m, there is no significant phase variation when using the DGPS error solution (Fig. 5a). Only the absolute position errors for the repeat-pass scenario with a standard deviation of $\sigma_B = 4.3$ cm yield a remarkable phase signature with a strong variation in Azimuth (Fig. 5b). This is due to the scattering of the error vector after each time step ($dt=1s$) which causes a jump/offset in the phase cycle. In Range direction, we also measure a phase gradient of about 0.1 rad from Near Range (NR) to Far Range (FR). With an altitude of ambiguity of about $h_a=1035$ m at mid-swath (Eq. 15) and a radar/incidence look angle of about 36 degrees, this phase gradient corresponds to a change in terrain elevation

$$dh = h_a \cdot d(\Delta\Phi)/2\pi \quad (23)$$

of roughly 1.7 m.

6. Conclusion

It has been proven that the estimated baseline performance of a multistatic SAR interferometer in a close formation flight fulfills the DTED-3 relative height accuracy requirement (< 2 m linear point-to-point error at 90% probability) for most of the baseline constellations if geodetic grade dual-frequency GPS receivers onboard the SAR satellites are used for relative positioning.

If a single-frequency GPS receiver is used for differential positioning, the direct elimination of differential ionospheric delay of the GPS signals is no longer possible. Furthermore, the resolution of the carrier-phase ambiguities is complicated and becomes even more difficult and inaccurate with increasing spatial separation. Therefore, the performance of the processing scheme using code and phase measurements of only one GPS signal must be investigated with respect to varying and long baselines (i.e., > 1 km)

Although we believe that the dual-frequency GPS baseline performance will also fulfill the DTED-3 horizontal accuracy requirements, a further analysis should clarify the propagation of the total 3-D baseline error vector to the height and horizontal circular bias.

Finding a correct trade-off between low topographic height bias, good coherence of the SAR data, and optimal terrain circumstances such as relief, vegetation, as well as temporal decorrelation will be the main objective for the planning of a future multistatic SAR mission. Using a dual-frequency GPS receiver as an operational tool for POD and relative navigation will help to solve the most problems related to a formation flight in a low Earth orbit (LEO) and ensures 2-D baseline accuracies smaller than 2 mm.

Acknowledgments

The authors would like to thank Michael Eineder from the DLR Remote Sensing Technology Institute (IMF) for his kind help in generating the interferograms. The study presented in this paper has mainly been carried out in the framework of a finished research fellowship awarded by the Deutsche Forschungsgemeinschaft (DFG). The first author gratefully acknowledges this grant.

References

- [1] Zebker HA, Farr T, Salazar R, and Dixon T, "Mapping the World's Topography Using Radar Interferometry: The TOPSAT Mission", Proc IEEE 82(12), pp. 1774-1786, 1994
- [2] Moreira A, Krieger G, and Hajnsek I, "TanDEM-X: A TerraSAR-X Add-On Satellite for Single-Pass SAR Interferometry" Proc International Geoscience And Remote Sensing Symposium (IGARSS), Anchorage, Sep 2004
- [3] Rodriguez E, and Martin JM, "Theory and Design of Interferometric Synthetic Aperture Radars", Proc IEE 139(2), pp. 147-159, 1992
- [4] Hanssen RF, "Radar interferometry: Data interpretation and error analysis", Kluwer Academic Publisher, Dordrecht Boston London, 2001
- [5] Krieger G, Fiedler H, Mittermayer J, Papathanassiou K, and Moreira A, "Analysis of Multistatic Configurations for Spaceborne SAR Interferometry", Proc Radar, Sonar, Navigation 150(3), pp. 87-96, 2003
- [6] Tapley BD, Bettadpur S, Ries JC, Thompson PF, and Watkins M, "GRACE Measurements of Mass Variability in the Earth System", Science 305(5683), pp. 503-505, 2004
- [7] Kroes R, and Montenbruck O, "Spacecraft Formation Flying", GPS World, pp. 37-42, 2004
- [8] D'Amico S, and Montenbruck O, "Proximity Operations of Formation Flying Spacecraft using an Eccentricity/Inclination Vector Separation", AIAA Journal of Guidance, Control and Dynamics, in press, 2006
- [9] Case K, Kruizinga G, and Wu S, "GRACE Level 1B Data Product User Handbook", JPL Publication D-22027, Jet Propulsion Laboratory, Pasadena, 2002
- [10] Montenbruck O, Van Helleputte T, Kroes R, and Gill E, "Reduced Dynamic Orbit Determination using GPS Code and Carrier Measurements", Aerospace Science and Technology 9(3), pp. 261-271, 2004
- [11] Kroes R, Montenbruck O, Bertiger W, and Visser P, "Precise GRACE baseline determination using GPS", GPS Solutions 9, pp. 21-31, DOI 10.1007/s10291-0123-5, 2004